Polym. Bull. (2010) 65:719–730
DOI 10.1007/s00289-010-0321-y

ORIGINAL PAPER

Effects of [Bmim]OH on structure and conductive properties of alkaline PVA/[Bmim]OH membranes

Xiuling Zhu · Biao Wang · Huaping Wang

Received: 1 March 2010 / Revised: 30 May 2010 / Accepted: 10 June 2010 /
Published online: 25 June 2010

Abstract A series of alkaline polyvinyl alcohol/1-ethyl-3-methylimidazolium hydroxide (PVA/[Bmim]OH) electrolyte membranes were developed via a direct blending and solution casting method. The structure and conductive properties of PVA/[Bmim]OH membranes with various concentrations of [Bmim]OH were systematically studied using X-ray diffraction (XRD), scanning electron microscopy (SEM), energy dispersive X-ray spectroscopy (EDX), attenuated total reflectance Fourier-transform infrared (ATR-FTIR), tensile-strength analysis, and AC impedance spectroscopy. When blended, the PVA/[Bmim]OH membrane exhibited superior ionic conductive and the maximum ionic conductivity was found around 0.0196 S cm^{-1} when the weight ratio of [Bmim]OH to PVA was 2.0. A model was proposed to illustrate the structure of PVA/[Bmim]OH membranes and the effect of [Bmim]OH on the ionic conductivity of the PVA matrix. The results and the model indicated that the addition of [Bmim]OH could significantly improve the electrochemical properties of the membranes, which is a promising candidate for direct methanol fuel cells (DMFCs) applications.

Keywords Alkaline electrolyte membrane · Ionic liquid · Polyvinyl alcohol · Ionic conductivity

Introduction

Direct methanol fuel cells (DMFCs) are promising environmentally friendly and efficient power sources for vehicles, buildings, and some portable electronic

X. Zhu · B. Wang (✉) · H. Wang
State Key Laboratory for Modification of Chemical Fiber and Polymer Materials,
College of Materials Science and Engineering, Donghua University, Shanghai 201620,
People's Republic of China
e-mail: wbiao2000@dhu.edu.cn

devices, such as computers, and mobile communication equipments [1–4]. Polymer electrolyte membranes, the principal component in DMFCs, dually act as a separator between the catalyst layers to prevent permeation of the methanol fuel and as an electrolyte to transport charges throughout the fuel cell. Based on their transport charge, the electrolyte membranes could be divided into the proton exchange membranes (PEMs) and alkaline anion exchange membranes (AEMs) [2, 5, 6]. AEMs are the much more advanced and promising electrolyte membranes, as a result of their high methanol oxidation rate, low methanol permeability, and high power densities which can be obtained with low catalyst loadings [2, 4, 6] or cheaper non-noble metal catalysts [7].

Recently, much advancement has been made toward the development of AEMs materials [8, 9]. Among these, polyethylene oxide (PEO)-based membrane incorporated KOH showed attractive characteristics of voltage versus current density when it was used in alkaline fuel cells [10, 11]. However, the high crystallinity of PEO membranes hinders further improvement in the current density of fuel cells [2, 12]. Yang et al. chose PVA as the polymer matrix and reported an alkaline polyvinyl alcohol/tetraethyl ammonium chloride (PVA/TEAC) blended polymer electrolytes [13, 14], whose ionic conductivity was explored up to 10^{-2} S cm^{-1} at ambient temperature. These membranes, however, easily degraded, limiting their further application in a fuel cell system.

Besides modifying membrane materials, the use of ionic liquids as electrolytes in the membrane system shows the promising perspective, because ionic liquids have been utilized as a novel reaction media in batteries, solar cells, and fuel cells operations [15–19]. In the applications of alkaline fuel cells, ionic liquids also exhibit their ideal properties, such as high thermal stability, low volatility, low melting points, and co-solvent miscibility and so on. Therefore, in order to combine the aforementioned advantages of AEM and ionic liquids, it is essential to modify PVA with an alkaline ionic liquid to obtain the alkaline electrolyte membranes for DMFCs.

In the present study, a basic ionic liquid, 1-ethyl-3-methylimidazolium hydroxide ([Bmim]OH) was applied to prepare alkaline PVA/[Bmim]OH blended polymer electrolytes membranes. The influences of [Bmim]OH and its concentration on the structure, morphology, and conductive properties of the membranes have been investigated.

Experimental

Commercially available PVA and [Bmim]OH were used in this research. PVA ($(CH_2CHOH)_n$, polymerization degree: $n = 1750 \pm 50$) was supplied by Sinopharm Chemical Reagent Co. Ltd, and [Bmim]OH ($C_8H_{16}N_2O$) was provided by Shanghai Chengjie Chemical Reagent Co. Ltd. Upon receipt, PVA was dissolved in de-ionized water under magnetic stirring for 3 h at 95 °C to obtain the solution with the concentration of 10 wt%. [Bmim]OH was dissolved in the previous PVA solutions with the various weight ratios of [Bmim]OH to PVA as shown in Table 1. The procedure was allowed to proceed for 2 h at 95 °C under magnetic stirring.

Table 1 Weight ratio of each sample group

Sample groups	[Bmim]OH:PVA (weight ratio)
BP-1	0.5
BP-2	1.0
BP-3	1.5
BP-4	2.0
BP-5	2.5

Then, the PVA/[Bmim]OH solutions were sonicated for 1 h to remove air bubbles, and the final solutions were casted onto glass plates followed by drying for 12 h at room temperature.

The surface morphologies of PVA/[Bmim]OH polymer membranes were investigated by a JSM-5600LY scanning electron microscope (SEM). Before the SEM observation, all samples were deposited on a layer of Au. The crystal structures of PVA/[Bmim]OH membranes were examined by using Philips X'Pert X-ray diffraction (XRD) and energy dispersive X-ray (EDX). In addition, attenuated total reflection (ATR)-FTIR spectroscopy was employed to characterize the chemical composition of pure PVA and PVA/[Bmim]OH membranes. Infrared spectra of all membranes were obtained by the ATR-FTIR spectroscope (Nicolet NEXUS-670, USA) at 25 °C with a midrange of 400–4000 cm^{-1}.

Water uptake and swelling of the membranes at 60 °C was determined by batch experiments. Before measurement, all PVA/[Bmim]OH polymer membranes were dried in a vacuum oven at 80 °C for 5 h. And then each membrane were weighed and immersed in deionized water for 2 days 60 °C. The weights of the swollen membranes were measured and the water uptake (WU, wt%) was evaluated by following equation [20]:

$$\mathrm{WU} = \frac{W_{\mathrm{wet}} - W_{\mathrm{dry}}}{W_{\mathrm{dry}}} \times 100\% \tag{1}$$

where W_{wet} is the weight of the water-swollen membranes and W_{dry} is the weight of dry membranes. The dimensional swelling (DS) membranes were investigated by volume change as following:

$$\mathrm{DS} = \frac{V_{\mathrm{wet}} - V_{\mathrm{dry}}}{V_{\mathrm{dry}}} \times 100\% \tag{2}$$

where V_{wet} and V_{dry} are the volume of the water-swollen and dry membranes, respectively.

Since possible harsh processes could not be completely avoided during assembling of the fuel cell and stack construction, it is indispensable that the membrane should possess good mechanical properties. The tensile strength of membranes was tested with a micro-controlled omnipotent mechanic test machine (WDW3020), in which the specimen was supported by a pair of fixture assemblies. All samples were cut into the size of 40 mm × 10 mm × 0.12 mm.

The OH^- ionic conductivity measurements of the alkaline PVA/[Bmim]OH electrolyte membranes were investigated by AC impedance method using a CHI650 galvano-chemistry system. The membranes, with a thickness of 0.12 mm, were sandwiched between a pair of circular graphite electrodes, whose diameters were 0.40 cm, and the testing frequencies were ranging from 0 to 10^5 Hz. The ionic conductivity of the membrane (σ) can be calculated from the following equation:

$$\sigma = L/(R_b \times A) \tag{3}$$

where

L is the thickness of the membrane (cm)
A is the area of membrane sandwiched between the graphite electrodes (cm^2)
R_b is the membrane resistance value (ohm) from the AC impedance data

Results and discussions

Structure and morphology analysis

The XRD patterns for pure PVA membrane and PVA/[Bmim]OH membranes are shown in Fig. 1. The PVA membrane reveals a semi-crystalline structure with a well-defined peak at 2θ of 20° and a less intense peak at 40° [21]. Since the addition of [Bmim]OH impacts the original structure of PVA crystalline, the intensity of PVA peaks are significantly weakened (see curve of BP-1 in Fig. 1). It is also can be detected in the figure that with the increase of [Bmim]OH concentration, the crystalline peaks of PVA matrix become less defined and split from one sharp peak into two smaller smooth peaks at 20° and around 23°. This suggests that the addition of the [Bmim]OH destroys the crystalline domain of the PVA matrix, thereby increasing the motion of PVA chains, losing the polymer chain packing and decreasing chain rigidity. The increased amorphous region makes the local chain

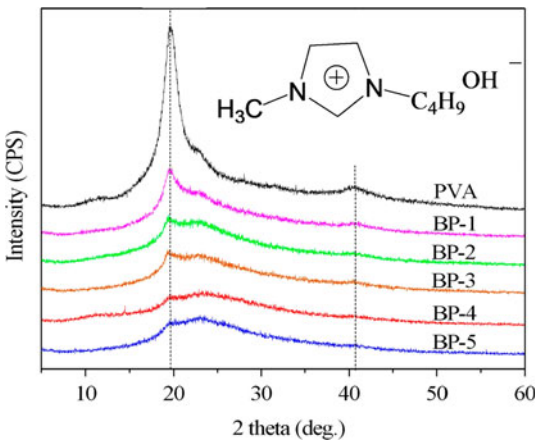

Fig. 1 XRD patterns for PVA and PVA/[Bmim]OH membranes, and the inset shows the chemical formula of [Bmim]OH

segmental motion more flexible [22], which probably contribute into producing a much higher ionic conductivity.

Since the physical properties of the membranes varied with [Bmim]OH concentrations, it was expected that the surface morphology of the PVA and the PVA/[Bmim]OH membranes would also vary (Fig. 2). Both the surfaces of PVA and BP-1 are smooth and homogeneous, as shown in Fig. 2a, b, and it is hardly to find out any significant difference in the morphology between the two membrane samples. However, the surface morphology of the PVA/[Bmim]OH membranes change dramatically as the [Bmim]OH concentration increasing, and the most notable changes are observed on the images of BP-2 and BP-3 (Fig. 2c, d). In Fig. 2c for the specimen of BP-2, some obvious light field phases are uniformly distributed on the surface of the membrane, and the diameter distributions of the light field phases are shown in Fig. 3a. In this figure, the histogram illustrates the occurrence frequency versus the diameters of the light field phases, while the red curve shows the percentage of the light field phases whose diameter are smaller than the corresponding horizontal coordinate. Calculated diameters of most light field phases are around 5–7 μm. In order to analyze the structure of these light field phases and the distribution of [Bmim]OH adequately, EDX mapping for carbon and nitrogen elements were implemented for BP-2 samples (Fig. 4), with Fig. 4a showing a SEM enlarged view for a couple of light field phases from Fig. 2c. In the EDX mapping image, the highlighted bright dots represent high elemental concentration with a red stain for carbon and a green stain for nitrogen. There is a low concentration of carbon elements in the light field phases according to Fig. 4b; while the nitrogen element exhibits a relatively high concentration in the light field phases (see Fig. 4c). Moreover, the observation of nitrogen supports the existence of the [Bmim]OH in the membranes and the distribution of nitrogen matching the distribution of the [Bmim]OH through the membrane. Therefore, the light field phases in BP-2 can be considered as the [Bmim]OH-rich areas, while the

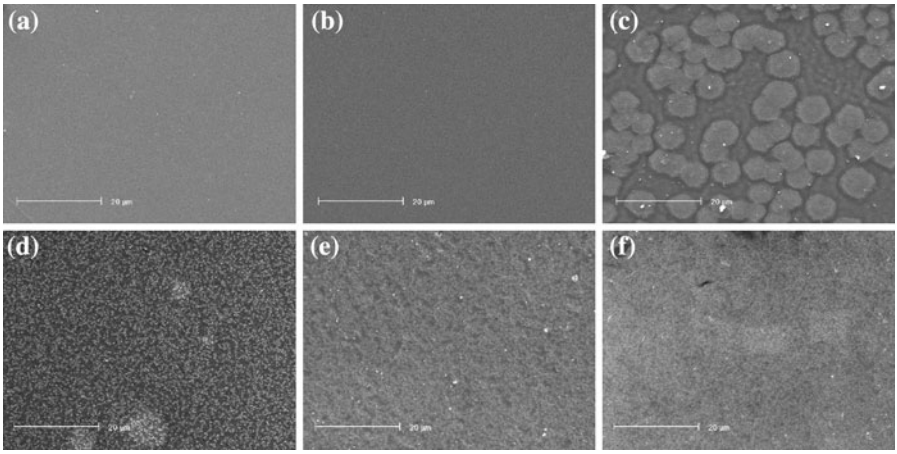

Fig. 2 SEM micrographs for surfaces of membranes. **a** PVA membrane, **b** BP-1, **c** BP-2, **d** BP-3, **e** BP-4, **f** BP-5

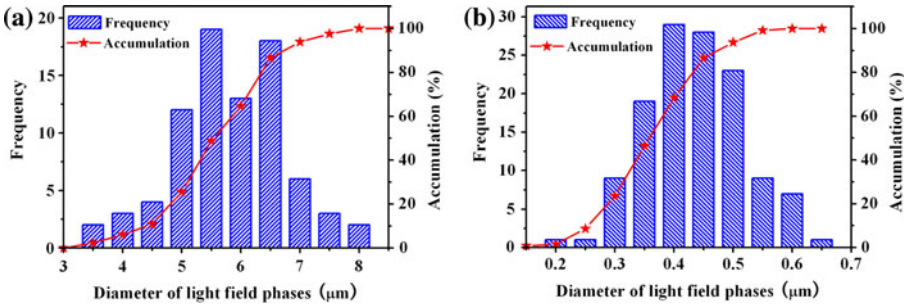

Fig. 3 Diameter distribution of light field phases in **a** BP-2 and **b** BP-3

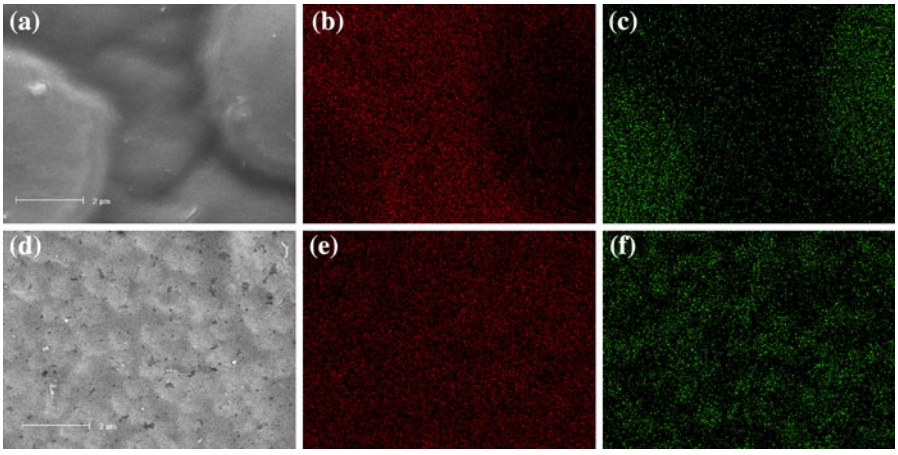

Fig. 4 **a** SEM enlarged views from Fig. 2c. **b** and **c** are EDX elemental distribution for elements of carbon and nitrogen, respectively. **d** SEM enlarged views from Fig. 2e. **e** and **f** are EDX elemental distributions for elements of carbon and nitrogen, respectively

others are PVA-rich areas. The average diameter (d_m) can be obtained according to the equation of weighted arithmetic mean defined as:

$$d_m = \frac{\sum_i n_i d_i}{\sum_i n_i} \tag{4}$$

where d_i is diameter, and n_i is the frequency of corresponding d_i. Using this equation, the d_m of [Bmim]OH-rich light field phases in BP-2 is 16.00 μm.

When the weight ratio of [Bmim]OH to PVA increases to 1.5 (BP-3), the diameter of high-[Bmim]OH light field phases significantly decrease as shown in Fig. 2d. Figure 3b gives the light field phase size distribution. According to Eq. 2, the average diameter of the light field phases is 0.44 μm, which is one order of magnitude lower than that of BP-2. As opposed to BP-2, the fine light field phases for BP-3 are smoothly dispersed throughout the whole membrane. While for the

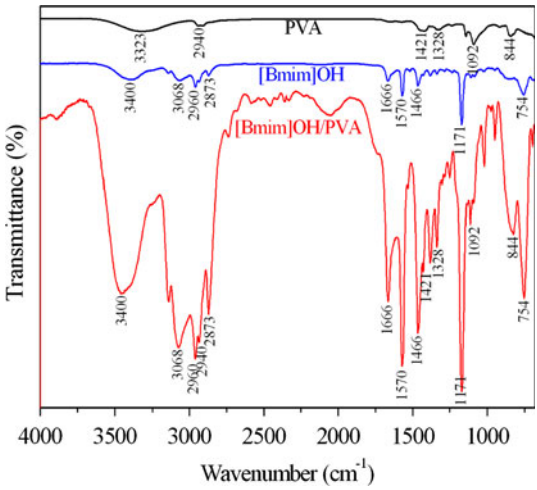

Fig. 5 ATR-FTIR spectrums for PVA, [Bmim]OH and PVA/[Bmim]OH membranes

sample of BP-4, there is no obvious agglomeration and micro-phase separation. Figure 4d illustrates the SEM enlarged view of Fig. 2e, which shows that the membrane has a uniform surface. According to the EDX mapping for carbon and nitrogen shown in Fig. 4e, f, respectively, the carbon and nitrogen elements are smoothly distributed throughout the membrane, suggesting the homogeneous blending of [Bmim]OH and PVA. In addition, the surface of BP-5 reveals similar morphology as BP-4, but there are some inhomogeneous agglomerations as shown in Fig. 2f.

The ATR-FTIR spectra of pure PVA, [Bmim]OH, and PVA/[Bmim]OH membrane (with the ratio of 2.0) are illustrated in Fig. 5. For pure PVA, the broad absorption peaks at 3323 and 1092 cm^{-1} correspond to –OH groups, and 2940 cm^{-1} corresponds to the stretching of C–H bonds. For the spectrum of [Bmim]OH, –OH transitions are detected as a broad peak at 3340 cm^{-1} and a very intensive peak at 1171 cm^{-1}. When compared with the spectra of the pure PVA membrane and [Bmim]OH, the spectrum of the PVA/[Bmim]OH membrane contains signals arising from each of the [Bmim]OH and pure PVA membrane components. This observation confirms that the PVA/[Bmim]OH membrane is a blend material rather than a composite.

Water uptake and swelling analysis

The results of water uptake and swelling of each PVA/[Bmim]OH membrane are shown in Table 2. As can be seen that both of the water uptake and the dimensional swelling are increasing with elevated ratio of [Bmim]OH to PVA, which could be attributed to the well-known hydrophilic property of the ionic liquids. However, the water plays a critical role on ionic conductivity properties of the membranes, which will be discussed in the following parts. On the other hand, the results indicated that all swellings of PVA/[Bmim]OH membranes are less than 10% except the BP-5 sample, suggesting negligible swelling at 60 °C.

Table 2 Water uptake and swelling of each PVA/[Bmim]OH membrane

Samples	Water uptake (%)	Dimensional swelling (%)
BP-1	7.32	4.19
BP-2	9.89	5.22
BP-3	13.77	7.87
BP-4	15.02	8.20
BP-5	20.33	11.04

Mechanical property analysis

Stress–strain tests were used to determine the mechanical properties of PVA/[Bmim]OH membranes. The stress–strain curves of the PVA/[Bmim]OH membranes with various concentrations of [Bmim]OH, as well as the commercial PVA are shown in Fig. 6. It can be obtained that both strength (20.47 MPa) and modulus (3.16 GPa) of PVA membrane are larger than those of all PVA/[Bmim]OH membranes, as the structure of PVA substrate changes upon addition of [Bmim]OH. The stress–strain curve of PVA/[Bmim]OH membranes exhibits nearly linear growing between stress and strain due to their ductile property. Although the tensile strength of the membranes noticeably decrease with the increase of [Bmim]OH concentration, it is observed to have an excellent strain-at-break value. Typically, when the concentration of [Bmim]OH is twice as much as PVA (BP-4 sample), the PVA/[Bmim]OH membrane illustrated a largest broken strain of 13.93%, with the calculated modulus is 0.39 GPa. From the XRD analysis in the previous subsection, it can be pointed out that the crystallinity of the PVA decreased and the amorphous phase increased because of the additional [Bmim]OH. Since PVA has a semi-crystalline structure, rapid crack propagation in the membrane would result in the brittle fracture property [23, 24]. While with addition of [Bmim]OH, the structure of membranes has been partially transformed from semi-crystalline to amorphous, resulting in improvement of their ductile property. On the other hand, as the weight ratio of [Bmim]OH to PVA larger than 2.0, both strength and broken strain dramatically decrease, suggesting that matrix phase of PVA is too limited to form a continuous phase.

Ionic conductivity analysis

To test the ionic conductivity of the PVA/[Bmim]OH membranes, AC impedance experiments were performed on each membrane, and the spectra are shown in Fig. 7. As expected, all spectra show a similar trend, which consisted of two well-defined regions, namely a high frequency and a low frequency range. The high frequency region is assigned to the ionic conduction process in the bulk of the membranes. While in the low frequency range, it could be related to the diffusion effect of the transport ions [25]. As is shown in Fig. 7, the conductivity property of all membranes vary with different concentration of [Bmim]OH. Table 3 gives the results of ionic conductivities (σ) calculated from Eq. 1 for all PVA/[Bmim]OH

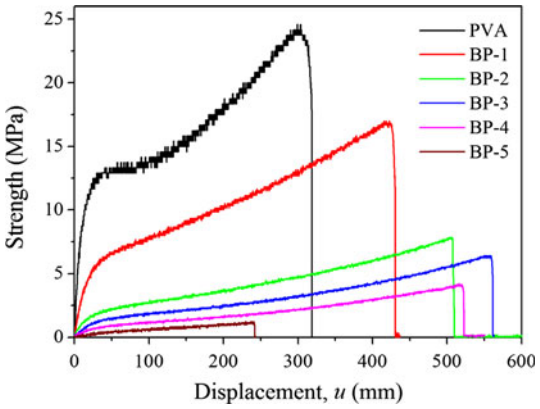

Fig. 6 The stress–strain curves of the PVA/[Bmim]OH membranes with various concentrations of [Bmim]OH, as well as the commercial PVA

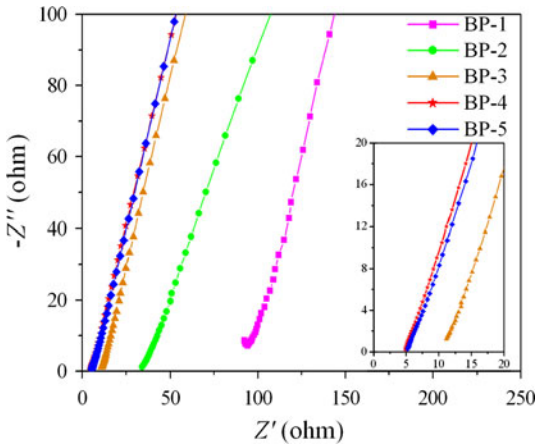

Fig. 7 AC spectra of PVA/[Bmim]OH membranes with different weight rates of [Bmim]OH:PVA

membranes at room temperature. As the ratio of [Bmim]OH to PVA increases, the R_b values decrease, and the corresponding values of the ionic conductivity are significantly enhanced. Due to the amorphous and homogenous structure, BP-4 has the lowest R_b value (4.87 ohm) and the best ionic conductivity (1.96×10^{-2} Scm^{-1}). Similarly, when compared with BP-4, the specimen of BP-5 has inferior conductivity due to the inhomogeneous structure, as shown in Fig. 2f. The improvement in conductivity property could be attributed to [Bmim]OH, which is a highly conductive material [16, 17]. When continuously dispersed throughout the membrane, the addition of [Bmim]OH destroys the crystalline domain of the PVA matrix, increases the amorphous phase, and produces a higher ionic transport.

Structure model

Based on the above results, we propose the structures of PVA and PVA/[Bmim]OH membranes shown in Fig. 8. As is generally accepted, the PVA is a semi-crystalline structure material consistent with the Fringed Micelle Model rather than a complete

Table 3 The ionic conductivities of the PVA/[Bmim]OH membranes with various concentration of [Bmim]OH at room temperature

Samples	R_b (ohm)	σ (S/cm)
BP-1	92.40	0.001033
BP-2	34.00	0.002809
BP-3	11.20	0.008526
BP-4	4.87	0.019608
BP-5	5.43	0.017586

crystal [26, 27], which is also confirmed by the XRD pattern of PVA membranes shown in Fig. 1. In this article, we develop a schematic description of the PVA, as shown in Fig. 8a. The pure PVA membranes consist of crystalline and amorphous phases. The crystalline phase is characterized as parallel PVA chains, while the amorphous phase is described as the irregular areas [26, 27]. By adding the basic ionic liquid [Bmim]OH, which introduces exchangeable anions, many physical properties of the membranes, such as the crystalline structure, dynamic mechanical property, thermal property, and morphology, change dramatically. Figure 8b, c gives the structure model of BP-2 and BP-4. In these models, the [Bmim]OH molecules, together with the residual water molecules, are freely distributed in the amorphous area of the PVA substrate, which is supported by the experimental data as the [Bmim]OH-rich light field phases (Figs. 2, 4). The water plays a critical role on charge transport mechanisms [28], as the anion transport in these membranes is intimately connected to the basic anionic bond network structural rearrangement in water associated with the [Bmim]OH. According to the EDX mapping image for nitrogen (Fig. 4f), the distribution of [Bmim]OH molecules is homogeneous between the PVA chains, which is also represented in the model in Fig. 8c. As shown in Fig. 8b, c, with the increase of the concentration of [Bmim]OH, the

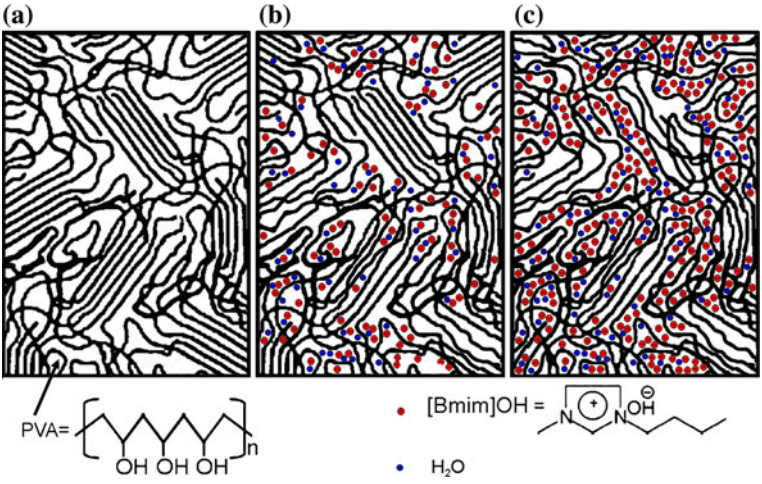

Fig. 8 Schematic description of structure models for PVA and PVA/[Bmim]OH membranes. **a** Pure PVA membranes, where the *black line* indicates the PVA chain. **b** BP-2. **c** BP-4

crystalline domain decreases, and the amorphous phase increases. On one hand, the decrease of the crystalline domain results in the decrease of the storage modulus and the enhancement of the strain. On the other hand, the increase of the concentration of the ionic liquid and the amorphous phase lead to the more flexible local chain segmental motion which produces a higher ionic transport. Theoretically, in order to produce membranes with higher quality, the higher storage modulus, more enhanced strain, and higher ionic transport are required. Unfortunately, these three factors cannot be obtained simultaneously by adding ionic liquids only. Therefore, compromise must be made. According to our experiments, the membrane with best quality can be produced under the concentration of 2.0.

Conclusion

A novel alkaline polymer electrolyte membrane was developed by direct blending of PVA and [Bmim]OH. Various concentrations of [Bmim]OH in the membranes were examined to analyze the effect of adding [Bmim]OH on the structure and ionic conductivity property of the membranes. With the blending of [Bmim]OH and PVA, the exchangeable anions from [Bmim]OH have been introduced into the PVA/[Bmim]OH membranes, and these membranes exhibit enhanced ionic conductive over other membranes proposed for DMFCs. Our results demonstrated that the structure of membrane depending on the concentration of [Bmim]OH is the principal factor that affects the mechanical and conductivity properties of the membranes. When the weight ratio of [Bmim]OH to PVA is 2.0, the membrane has the largest breaking elongation (13.93%) and the best ionic conductivity (1.96×10^{-2} S cm^{-1}). To better understand the behavior of these membranes, structural models for both PVA and PVA/[Bmim]OH membranes have been proposed on the molecular scale.

Acknowledgments This study was financially supported by the Natural Science Foundation of Shanghai, China (No.09ZR1401500), the project of the Action on Scientists and Engineers to Serve Enterprises (2009GJE20016), the Scientific Research Foundation for the Returned Overseas Chinese Scholars (Ministry of Education), the Cultivating Project of the Key Laboratory of High Performance Fibers and Products (Donghua University, Ministry of Education), Shanghai Leading Academic Discipline Project (B603) and Program of Introducing Talents of Discipline to Universities (No. 111-2-04). The authors thank Dr. Rachel L. Behrens and Matthew A. Rigsby from the University of Illinois at Urbana-Champaign for suggesting on writing. And also thank Dr. J. Li from National Institute for Materials Science of Japan for valuable discussion.

References

1. Steele BCH, Heinzel A (2001) Materials for fuel-cell technologies. Nature 414:345–352
2. McLean GF, Niet T, Prince-Richard S, Djilali N (2002) An assessment of alkaline fuel cell technology. Int J Hydrogen Energy 27:507–526
3. Danks TN, Slade RCT, Varcoe JR (2003) Alkaline anion-exchange radiation-grafted membranes for possible electrochemical application in fuel cells. J Mater Chem 13:712–721
4. Varcoe JR, Slade RCT, Lam How Yee E (2006) An alkaline polymer electrochemical interface: a breakthrough in application of alkaline anion-exchange membranes in fuel cells. Chem Commun 1428–1429

5. Gu S, He G, Wu X, Guo Y, Liu H, Peng L, Xiao G (2008) Preparation and characteristics of crosslinked sulfonated poly(phthalazinone ether sulfone ketone) with poly(vinyl alcohol) for proton exchange membrane. J Membr Sci 312:48–58
6. Varcoe JR, Slade RCT (2005) Prospects for alkaline anion-exchange membranes in low temperature fuel cells. Fuel Cells 5:187–200
7. Lu SF, Pan J, Huang AB, Zhuang L, Lu JT (2008) Alkaline polymer electrolyte fuel cells completely free from noble metal catalysts. Proc Natl Acad Sci USA 105:20611–20614
8. Clark TJ, Robertson NJ, Kotalik HA, Lobkovsky EB, Mutolo PF, Abruna HD, Coates GW (2009) A ring-opening metathesis polymerization route to alkaline anion exchange membranes: development of hydroxide-conducting thin films from an ammonium-functionalized monomer. J Am Chem Soc 131:12888–12889
9. Tang DP, Pan J, Lu SF, Zhang L (2010) Alkaline polymer electrolyte fuel cells: principle, challenges, and recent progress. Sci China Chem 153:357–364
10. Yang CC, Lin SJ (2002) Alkaline composite PEO-PVA-glass-fibre-mat polymer electrolyte for Zn-air battery. J Power Sources 112:497–503
11. Vassal N, Salmon E, Fauvarque JF (2000) Electrochemical properties of an alkaline solid polymer electrolyte based on P(ECH-co-EO). Electrochim Acta 45:1527–1532
12. Sekhon SS, Krishnan P, Singh B, Yamada K, Kim CS (2006) Proton conducting membrane containing room temperature ionic liquid. Electrochim Acta 52:1639–1644
13. Yang CC, Wu GM, Lin SJ (2006) Alkaline blend polymer electrolytes based on polyvinyl alcohol (PVA)/tetraethyl ammonium chloride (TEAC). J Appl Electrochem 36:655–661
14. Yang CC, Lin CT, Chiu SJ (2008) Preparation of the PVA/HAP composite polymer membrane for alkaline DMFC application. Desalination 233:137–146
15. Lee SH, Kim JK, Cheruvally G, Choi JW, Ahn JH, Chauhan GS, Song CE (2008) Electrochemical properties of new organic radical materials for lithium secondary batteries. J Power Sources 184: 503–507
16. Kan HC, Tseng MC, Chu YH (2007) Bicyclic imidazolium-based ionic liquids: synthesis and characterization. Tetrahedron 63:1644–1653
17. Zang H, Wang M, Cheng BW, Song J (2009) Ultrasound-promoted synthesis of oximes catalyzed by a basic ionic liquid [bmIm]OH. Ultrason Sonochem 16:301–303
18. Krossing I, Slattery JM, Daguenet C, Dyson PJ, Oleinikova A, Weingartner H (2006) Why are ionic liquids liquid? A simple explanation based on lattice and solvation energies. J Am Chem Soc 128:13427–13434
19. Lee JS, Nohira T, Hagiwara R (2007) Novel composite electrolyte membranes consisting of fluorohydrogenate ionic liquid and polymers for the unhumidified intermediate temperature fuel cell. J Power Sources 171:535–539
20. Qiao JL, Hamaya T, Okada T (2005) Chemically modified poly(vinyl alcohol)-poly(2-acrylamido-2-methyl-1-propanesulfonic acid) as a novel proton-conducting fuel cell membrane. Chem Mater 17:2413–2421
21. Upadhyay DJ, Bhat NV (2004) Pervaporation studies of gaseous plasma treated PVA membrane. J Membr Sci 239:255–263
22. Yang CC, Lin SJ, Wu GM (2005) Study of ionic transport properties of alkaline poly(vinyl) alcohol-based polymer electrolytes. Mater Chem Phys 92:251–255
23. Wan Y, Creber KAM, Peppley B, Bui VT (2006) Chitosan-based electrolyte composite membranes II. Mechanical properties and ionic conductivity. J Membr Sci 284:331–338
24. Shimizu S, Aiki Y, Ikake H, Kurita K (1999) Small-angle X-ray scattering from poly(methylmethacrylate) in aqueous solutions of t-butyl alcohol. J Polym Sci B Polym Phys 37:2195–2199
25. Wu GM, Lin SJ, Yang CC (2006) Preparation and characterization of high ionic conducting alkaline non-woven membranes by sulfonation. J Membr Sci 284:120–127
26. Rosen SL (1993) Fundamental principles of polymeric materials. Wiley, New York, pp 40–41
27. Sugiyama M, Maeda Y (1995) Small-angle neutron-scattering study of annealed and stretched PVA-films. J Phys Soc Jpn 64:1002–1010
28. Shen CC, Joseph J, Lin YC, Lin SH, Lin CW, Hwang BJ (2008) Modifying microphase separation of PVA based membranes for improving proton/methanol selectivity. Desalination 233:82–87